

# Role of Molecular Structure in the Production of Water-Soluble Species by Photo-oxidation of Petroleum

Martha L. Chacón-Patiño,\* Sydney F. Niles, Alan G. Marshall, Christopher L. Hendrickson, and Ryan P. Rodgers\*

Cite This: *Environ. Sci. Technol.* 2020, 54, 9968–9979

Read Online

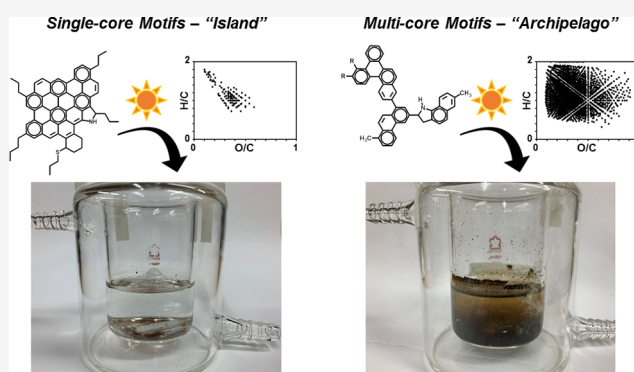
ACCESS |

Metrics & More

Article Recommendations

Supporting Information

**ABSTRACT:** Asphaltenes are high-boiling and recalcitrant compounds that are generally minor components of crude oil (~0.1–15.0 wt %) but dominate the composition of heavily weathered spilled petroleum. These solid residues exhibit a high structural complexity, comprised of polycyclic aromatic hydrocarbons (PAHs) that are a mixture of single-core (island) and multicore (archipelago) structural motifs. The mass fraction of each motif is sample-dependent. Thus, knowledge of a potential structural dependence (single- versus multicore) on the production of water-soluble species from asphaltene samples is key to understanding the contribution of photochemically generated dissolved organic matter from oil spills. In this work, asphaltene samples with enriched mass fractions of either island (single-core) or archipelago (multicore) structural motifs are photo-oxidized on artificial seawater by the use of a solar simulator. Molecular characterization of oil- and water-soluble photoproducts, conducted by Fourier transform ion cyclotron resonance mass spectrometry, reveals that island motifs exhibit very limited production of water-soluble species, and their oil-soluble products reflect the molecular composition of the starting material. Conversely, archipelago motifs yield a water-soluble compositional continuum of  $O_x$ ,  $S_xO_y$ , and  $N_xO_z$ , containing hydrocarbons species that exhibit the typical molecular fingerprint of dissolved organic matter (DOM). The lower carbon number and aromaticity of the archipelago-derived asphaltene photoproducts suggest the occurrence of photofragmentation (or photolysis) reactions. To investigate the possibility of the opposite reaction (photopolymerization), the photo-oxidation of small PAHs isolated from a low-boiling petroleum distillation cut was also performed. It yielded water-soluble compounds with carbon number and aromaticity up to 2-fold higher than the starting material, strongly suggesting that polymerization (addition reactions) occurs. Collectively, the results indicate that the presence of archipelago motifs and the occurrence of cracking/polymerization reactions are central in the production of dissolved organic matter from fossil fuels.



## INTRODUCTION

**Asphaltene Fate in Oil Spills.** As global petroleum transportation continues to rise, oil spills increasingly become a significant potential threat to marine and coastal ecosystems.<sup>1</sup> It is well documented that evaporation is the most critical process related to mass loss in most oil spills.<sup>2–4</sup> Light and medium crude oils can lose between 40 and 75% of their initial volume within the first month post spill; however, heavy petroleum feedstocks typically lose less than 10% of their initial spilled volume.<sup>5</sup> Nevertheless, after evaporation, the remnant material is enriched in the most refractory petroleum species, asphaltenes,<sup>6</sup> shown to concentrate in spilled heavy oils. Asphaltenes are defined as the petroleum fraction that is insoluble in *n*-heptane but soluble in toluene (Tol), well known for their significant concentration of heavy metals, sulfur-, oxygen-, and nitrogen-containing aromatic compounds relative to maltenes.<sup>7</sup> Asphaltenes are also central contributors to the stabilization of water-in-oil emulsions.<sup>8,9</sup> Previous works suggest

that asphaltenes are the main species that emulsify the water droplets trapped in the typical oil mousses produced after petroleum spills.<sup>10,11</sup> Importantly, asphaltenes in field samples are likely a mixture of oxidized native asphaltenes (originally present in the spilled oil) and photochemically produced “new” asphaltenes generated by weathering of originally heptane-soluble species (maltenes).

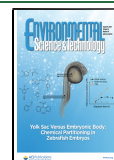
**Environmental Impact of Asphaltenes.** From the standpoint of petroleum production, refining, and environmental impact, asphaltenes are perhaps one of the most problematic crude oil fractions.<sup>12,13</sup> In oil production,

Received: February 25, 2020

Revised: July 14, 2020

Accepted: July 17, 2020

Published: August 4, 2020



asphaltenes are the major cause for clogging wells, pipelines, and surface facilities.<sup>14</sup> In refinery operations, asphaltenes trigger catalyst poisoning because they are enriched in heavy metals and serve as coke precursors.<sup>15</sup> In spills, asphaltenes constitute the most recalcitrant petroleum fraction and concentrate after the evaporation of the spilled oil has ceased.<sup>16</sup> Furthermore, because of their insignificant value as fuel, asphaltenes are commonly used for road paving.<sup>17,18</sup> Hot-mix asphalt is used for road paving and is a mixture of stone, sand, and petroleum distillation residues.<sup>19</sup> Several authors suggest that the use of distillation residues, known for their high asphaltene content, constitutes a significant source of pollutants in stormwater runoff, which potentially plays a crucial role in the contamination of drinking water supplies.<sup>20,21</sup> Thus, the potential environmental impacts of asphaltenes are not solely limited to oil spills.

Asphaltenes comprise between ~1.0 and 2.5% by weight of asphalt binders and have a significant effect on the asphalt properties, such as its propensity to harden.<sup>22,23</sup> Since asphaltenes consist of structural motifs comprised of polycyclic aromatic hydrocarbons (PAHs),<sup>24,25</sup> it is plausible that paved roads can leach toxic hydrocarbons.<sup>26</sup> Recent works demonstrate that asphalt can produce dissolved organic carbon (DOC) in the environment through rainfall wash and runoff. For instance, Xue et al.<sup>27</sup> studied the leaching behavior of aged asphalt mixtures and found DOC concentrations between ~4 and 24 mg/L. The authors determined that laboratory-scale asphalt aging, induced by thermal stress, pressure, and ultraviolet irradiation, increases the DOC leachability by a factor of ~5, compared to nonaged asphalt mixtures.<sup>27</sup> Other studies conducted by Hallberg, Zhao, Norin, and Sansalone et al.<sup>28–31</sup> demonstrate that the leached DOC from asphalt is enriched in PAHs, heavy metals, and oxygen-containing compounds with the typically reported molecular composition of dissolved organic matter (DOM, up to ~20 oxygen atoms per molecule, molecular weight between 200 and 700 g/mol, and H/C ratios from 0.5 to 2.0).<sup>32,33</sup> Additional reports suggest that soils near and under paved roads exhibit a higher concentration of PAHs, such as anthracene and pyrene, than those located away from roads and highways.<sup>34</sup> It is important to highlight that apart from asphalt, another source of PAHs in locations near roads is the incomplete combustion of fossil fuels.<sup>35</sup>

**Asphaltene Chemistry is Elusive.** Because asphaltenes are believed to be the most recalcitrant species in oil spills and are a critical component of hot-mix asphalt, understanding their transformation by weathering processes is important to determine environmental impact and subsequent remediation. However, the story of the molecular composition of asphaltenes is plagued with controversy. The reason is simple: asphaltenes are one of the most complex naturally occurring mixtures, with 100 000+ unique molecular formulas determined by mass spectrometry (MS) (each of which is the sum of a myriad of isomers), and their complete characterization has been impeded by their self-aggregation nature. Before 2013, the results regarding asphaltene characterization by mass spectrometry, which focused on whole/unfractionated samples, suggested that the asphaltene structure consisted of a single PAH, with more than ~7 fused rings and alkyl side chains, known as single-core or island motif.<sup>36–38</sup> However, the sole dominance of island structures is inconsistent with asphaltene behavior under thermal stress (refinery processes) and the emulsifying properties of asphalt films in the environment.<sup>13</sup>

Chacón-Patiño et al.<sup>39</sup> reported asphaltene fractionation by extrography with silica gel as the adsorbent. The method yields

asphaltene fractions enriched in single-core (island) or multi-core motifs (archipelago). In extrography, asphaltenes are adsorbed on silica gel with a mass loading of ~1 wt %. The mixture is dried and then extracted in a Soxhlet apparatus by two major solvents: acetone and the mixture of toluene/tetrahydrofuran/methanol (Tol/THF/MeOH). Extrography separation involves the adsorption of the most polarizable compounds of asphaltenes on the active silanol groups of silica gel, whereas the least polarizable molecules are weakly retained within the silica pores. The initial extraction with acetone allows the separation of highly aromatic compounds, weakly adsorbed on the silica gel, because the dominant intermolecular forces of acetone consist of dipole–dipole interactions (also dominant in alkyl-deficient polycyclic aromatic hydrocarbons). The later extraction with toluene/THF/MeOH, with predominant hydrogen bonding interactions, yields a fraction with abundant N- and O-containing compounds.<sup>39</sup> The mass spectral analyses of whole/unfractionated asphaltene samples preferentially reveal species that ionize efficiently by atmospheric pressure photoionization (APPI) and are enriched in single-core/island compounds.<sup>1</sup> Furthermore, the acetone extrography fraction is comprised of easy-to-ionize single-core compounds that resemble the composition of the whole asphaltene sample. Their initial extraction enables the analysis of asphaltene species that are more difficult to ionize (toluene/THF/MeOH fraction), which are not accessed in the analysis of the unfractionated sample. This later fraction contains abundant structural motifs that consist of several smaller aromatic cores linked by covalent bridges, known as multicore or archipelago, which are challenging to ionize in atmospheric pressure photoionization and detect by MS, in part, because of their stronger aggregation tendencies. Recent studies demonstrate that the ratio of island to archipelago is sample-dependent and correlates with asphaltene behavior in refinery processes;<sup>40,41</sup> asphaltene samples enriched in island motifs are resistant to transformation by thermal stress, whereas samples with a high content of archipelago species can yield abundant hydrocarbon, oxygen, nitrogen, and sulfur-containing 1–5 ring PAHs when pyrolyzed.<sup>40</sup>

This work focuses on the transformation of asphaltenes in a solar simulator microcosm and the role of structural motifs in the production of water-soluble oxidized species. The use of a solar simulator has been previously demonstrated to mimic photo-oxidation processes in the environment, because photo-irradiated products from microcosms resemble weathered products identified in field samples.<sup>42–44</sup> For this purpose, whole samples and extrography fractions from Wyoming deposit (island-dominant) and Athabasca bitumen (archipelago-dominant) asphaltenes were dissolved in toluene and photo-oxidized on artificial seawater. Asphaltenes are denser than seawater (>1.10 kg/m<sup>3</sup>); however, asphaltene films floated in water due to the lower density of toluene (~0.87 kg/m<sup>3</sup>). Molecular-level characterization of oil-/water-soluble oxidation products, conducted by atmospheric pressure photoionization and electrospray ionization (ESI) coupled to 9.4 T Fourier transform ion cyclotron resonance mass spectrometry (FT-ICR MS), suggests that island/single-core motifs resist phototransformation because they exhibit limited production of water-soluble species as determined by mass spectrometry and their oil-soluble products have a molecular composition that resembles that of the starting material. Conversely, asphaltene samples enriched in archipelago/multicore motifs yield abundant water-soluble compounds that comprise a continuous distribution of O<sub>x</sub>

$S_1O_x$ ,  $S_2O_x$ ,  $N_1O_x$ , and  $N_1O_xS_1$  heteroatom classes with a typical molecular composition of petroleum-derived dissolved organic matter. It is important to note that the lower carbon number and decreased aromaticity of the archipelago-derived oxidation products suggest the occurrence of photofragmentation reactions. Furthermore, compounds with high oxygen content ( $>O_{10}$ ) exhibit higher carbon number and higher aromaticity than the photo-oxidation products with low oxygen content ( $<O_5$ ), suggesting two possible transformation pathways: compounds with a higher carbon number and a higher aromaticity, originally present in the starting material, could incorporate more oxygen atoms through photo-oxidation, and/or oxidized species with a lower carbon number, produced by photo-oxidation and photofragmentation, may undergo addition reactions to yield products with a higher molecular weight and more oxygen atoms. Thus, the incidence of polymerization reactions (addition reactions) was investigated by photo-oxidation of low-molecular-weight/nonpolar hydrocarbons, extracted from a low-boiling petroleum distillation cut (178–283 °C). The results indicate the production of water-soluble compounds with carbon number and aromaticity, as seen in the double bond equivalents (DBE) versus carbon number plots, 2-fold higher than the starting material, suggesting that polymerization reactions occur. For the first time, the results derived from separations and FT-ICR MS demonstrate that petroleum degradation by sunlight involves three key processes, known as photo-oxidation, photofragmentation, and polymerization, as suggested by Overton et al.<sup>45</sup> in 1980.

## ■ EXPERIMENTAL METHODS

**Materials.** High-performance liquid chromatography (HPLC) grade *n*-heptane ( $nC_7$ ), *n*-pentane ( $nC_5$ ), toluene (Tol), acetone, water, methanol (MeOH), and concentrated hydrochloric acid (HCl) were obtained from J.T. Baker and used as received. HPLC-grade tetrahydrofuran (no solvent stabilizer) was purchased from Alfa Aesar. Filter paper Whatman 2 and high-purity microglass fiber thimbles were used for filtration and Soxhlet extraction. Chromatographic grade silica gel ( $SiO_2$ ) was obtained from Fluka Analytical (70–230 mesh, pore size 60 Å) and used for extrography fractionation. Solid-phase extraction (SPE) cartridges of styrene–divinylbenzene (SDVB) polymer sorbents (Bond Elut Priority PolLutant (PPL)) were purchased from Agilent and used for extraction of water-soluble compounds.

**Preparation of Asphaltene Samples and Fractions Enriched in Island or Archipelago Motifs.** Asphaltenes were precipitated from Athabasca bitumen and Wyoming deposit crude oils following the standard method ASTM D 6560-12 with slight modifications.<sup>46</sup> In short, 10 mL of petroleum was mixed with 40 mL of  $nC_7$  under sonication and refluxed heating at 90 °C. The mixture was allowed to stand overnight; asphaltenes were collected by filtration and placed in a Soxhlet extractor equipped with  $nC_7$  for cleaning for 72 h. Asphaltenes were recovered by redissolution in hot toluene.

Asphaltene fractions enriched in island or archipelago motifs were obtained by a shortened version of the extrography method published elsewhere.<sup>39</sup> Briefly, asphaltenes were adsorbed on silica gel (1% mass loading) under a nitrogen atmosphere. The solid  $SiO_2$ /asphaltenes mixture was placed in a Soxhlet apparatus and extracted with acetone and toluene/THF/methanol (10:10:1). Asphaltene samples and the extrography fractions, labeled as “whole sample”, “acetone fraction”, and

“Tol/THF/MeOH fraction”, were dried and stored in amber-glass vials under nitrogen.

**Asphaltene Weathering in a Solar Simulation Microcosm.** Asphaltene solutions were prepared by dissolving 20 mg of asphaltene samples/fractions in 1 mL of toluene. The solutions were loaded onto autoclaved 70% artificial seawater (Instant Ocean Aquarium Systems, Inc., Mentor, OH) in a jacketed beaker coupled to a water chiller at 27 °C. Following asphaltene film/layer preparation, the beaker was placed in an ATLAS Suntest CPS solar simulator and subjected to irradiation for 24 h and stirred at 60 rpm. The period of irradiation is equivalent to 6 days of natural sunlight.<sup>44</sup> A dark control (with no irradiation) was prepared similarly; a thin asphaltene film on artificial seawater was prepared and the beaker was covered with aluminum foil and stirred for 24 h. Separation of water and oil phases was performed by filtration through a wet cellulose filter paper (HPLC-grade water/Whatman 2 filter paper). Oil phases (oxidized oil-soluble products) were stored in amber-glass vials under a nitrogen atmosphere for subsequent MS analysis.

**Extraction of Water-Soluble Compounds.** Water-soluble species, referred to as dissolved organic matter (DOM) or alternatively (in the current study) as petroleum-derived dissolved organic matter ( $DOM_{HC}$ ), were isolated by solid-phase extraction (SPE), as reported by Dittmar et al.<sup>47</sup> In short, water samples were acidified with HCl to pH 2 and Bond Elut Priority PolLutant (PPL) cartridges (styrene–divinylbenzene (SDVB) stationary phase) were conditioned with MeOH. Water samples were loaded onto the PPL cartridges at a rate of 20 mL/min and washed with acidified HPLC-grade water (pH 2) to remove salt derived from the artificial seawater. The cartridges were dried under a nitrogen atmosphere for 20 min, and water-soluble asphaltene-derived organic species were eluted with MeOH. The samples were stored in amber-glass vials at 4 °C for MS analysis.

**Molecular-Level Characterization by 9.4 T Fourier Transform Ion Cyclotron Resonance Mass Spectrometry.** Asphaltene samples, extrography fractions, and oil-soluble oxidation products were diluted in toluene to a final concentration of 50  $\mu\text{g/mL}$  prior to analysis by positive-ion (+) APPI coupled with a custom-built 9.4 T FT-ICR mass spectrometer.<sup>48</sup> The samples were directly infused at 50  $\mu\text{L/min}$  into a ThermoFisher ion max APPI source (ThermoFisher Scientific, San Jose, CA). The vaporizer temperature was 350 °C,  $N_2$  sheath gas was set at 50 psi, and auxiliary  $N_2$  flow, to prevent in-source oxidation, was 32 mL/min. Gas-phase neutrals were photoionized by an ultraviolet krypton lamp (10 eV, Syagen Technology, Inc., Tustin, CA). Ions were transferred to the mass spectrometer through a heated metal capillary operated at  $\sim 350$  °C/ $\sim 8.5$  mA. Water-soluble oxidation products were ionized by negative-ion (–) microelectrospray ionization (ESI). The samples were infused at 500 nL/min into a custom-built microelectrospray source, (50  $\mu\text{m}$  i.d. fused silica emitter) operated at 3000 V as previously described.<sup>42</sup> It is important to note that (+) APPI is the ionization technique of choice for the characterization of asphaltenes and oil-soluble products,<sup>49</sup> whereas (–) ESI is well suited for water-soluble compounds.<sup>50</sup> The ionization of water-soluble products by (+) APPI yielded no stable ion signal for data collection. The ions were analyzed by a custom-built 9.4 T FT-ICR mass spectrometer. Time-domain transients were collected and processed by customized Predator software. Ions were accumulated for 5–5000 ms in an external radio frequency octopole and collisionally cooled with helium prior to transfer to a dynamically harmonized FT-ICR

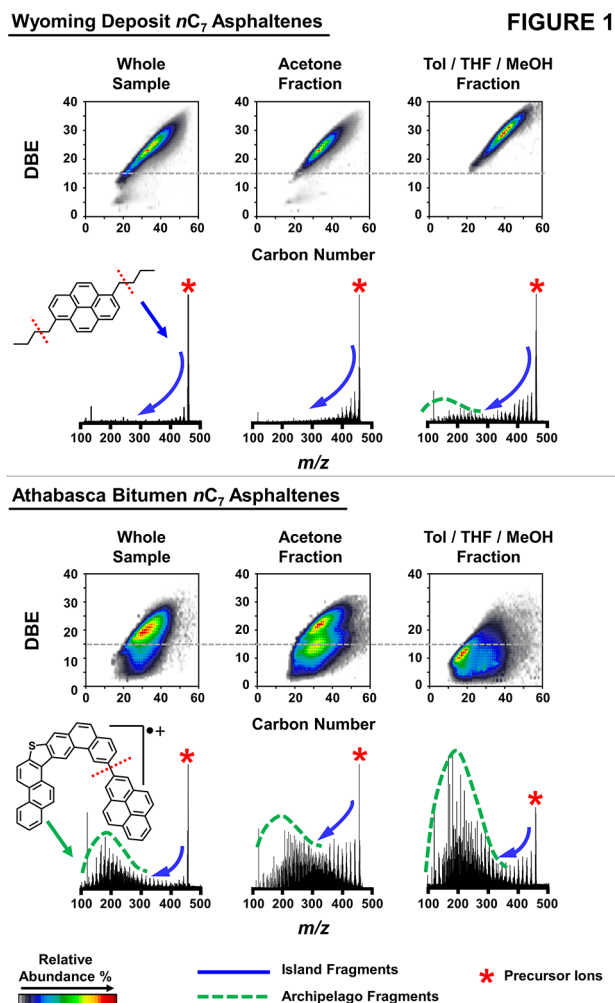
cell. Chirp excitation accelerated the ions to a detectable cyclotron radius.  $\sim 200$  time-domain transients were co-added, Hanning-apodized, and zero-filled before Fourier transform. The frequency was transformed to  $m/z$ ; the resulting mass spectra were internally calibrated by use of extended homologous alkylation series. PetroOrg Software enabled molecular formula assignment and data visualization.<sup>51,52</sup> For structural studies (tandem-MS), the ions were isolated by a mass-resolving quadrupole before external ion accumulation. The ions were fragmented by infrared multiphoton dissociation (IRMPD,  $\lambda = 10.6 \mu\text{m}$ , 40 W, 1000 ms irradiation, Synrad CO<sub>2</sub> laser, Mukilteo, WA).

## RESULTS AND DISCUSSION

**Asphaltenes from Diverse Geological Origins Exhibit Different Molecular Composition and Structure.** The work herein focuses on the role of molecular structure in asphaltene transformation into water-soluble species upon photo-oxidation in a solar simulation microcosm. Therefore, Wyoming deposit (single-core/island-dominant) and Athabasca bitumen (multicore/archipelago-dominant)  $n\text{C}_7$  asphaltenes were selected because they have previously been determined to exhibit different structural motifs and molecular compositions, accessed by FT-ICR MS and tandem-MS.<sup>40</sup> The results that reveal the structural motifs present in Wyoming and Athabasca bitumen asphaltenes are summarized in Figure 1.

Molecular formulas, assigned to the mass spectral peaks, derived from the FT-ICR MS analysis of whole samples and extrography fractions, were sorted by heteroatom classes (e.g., all of the formulas with C, H, and one N atom,  $\text{C}_x\text{H}_y\text{N}_1$ , comprise the  $\text{N}_1$  class), double bond equivalents (DBE = number of rings plus double bonds), and carbon number. The molecular formulas are represented in isoabundance-contoured plots of DBE versus carbon number, in which the color scale corresponds to the relative abundance. Figure 1 presents the combined compositional range, displayed as DBE versus carbon number plots, for the most abundant classes ( $>1\%$  of relative abundance) for whole Wyoming deposit (upper panel) and whole Athabasca bitumen (lower panel) asphaltenes and their acetone and Tol/THF/MeOH extrography fractions, accessed by positive-ion APPI 9.4 T FT-ICR MS. Figure 1 also presents structural information from infrared multiphoton dissociation (IRMPD, gas-phase fragmentation) followed by FT-ICR MS (tandem-MS). The fragmentation data reveals differences in asphaltene structure between the samples and fractions. Wyoming deposit asphaltenes (whole sample and fractions) present a compositional range dominated by highly aromatic compounds (DBE  $> 15$ ) with few carbon atoms in alkyl side chains (alkyl-deficient). The Wyoming tandem mass spectra feature a unique fragmentation pattern highlighted by a blue arrow, which starts at the  $m/z$  of the precursor ions ( $m/z$  450) and gradually decreases in relative abundance with decreasing  $m/z$ . This fragmentation profile is characteristic of island motifs, because ions lose carbon number (through dealkylation) but do not decrease in DBE because the single aromatic core remains intact during the dissociation. Therefore, the fragmentation behavior of Wyoming deposit asphaltenes demonstrates the dominance of island structures.

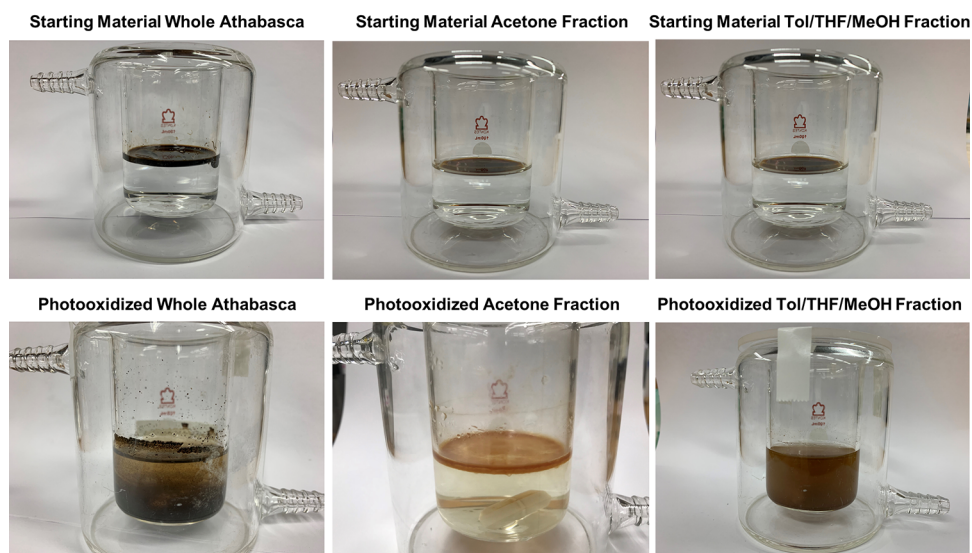
Conversely, Athabasca bitumen species exhibit a wider compositional range in terms of carbon number (increased alkylation) and atypical low DBE values (DBE 3–30) that suggest abundant species with smaller PAHs than Wyoming deposit. The fragmentation spectra reveal a pattern indicative of



**Figure 1.** Combined isoabundance-contoured plots of double bond equivalents (DBE) versus carbon number for compound classes with a relative abundance higher than 1% and fragmentation mass spectra for precursor ions isolated at  $m/z \sim 450$  for whole  $n\text{C}_7$  asphaltene samples and their acetone and Tol/THF/MeOH extrography fractions for Wyoming deposit (upper panel) and Athabasca bitumen (lower panel). Data derived from (+) APPI 9.4 T FT-ICR MS.

dealkylation (blue arrow, more evident for the acetone fraction); however, it also reveals a low-molecular-weight distribution (MWD) between  $m/z \sim 90$  and 300, highlighted by a green, dashed line. The low MWD is comprised of fragment ions with lower carbon number and lower DBE than the precursor ions, indicating the breakage of covalent linkages between small aromatic cores (archipelago) by tandem-MS, which yields one to five ring PAH fragments. Note that the acetone fractions from Wyoming deposit and Athabasca bitumen occupy a compositional range similar to those for the whole samples, due to the efficient ionization of the acetone species, and reveal a more pronounced dealkylation pattern (island motifs, blue arrow) than Tol/THF/MeOH. Therefore, the extrography fractionation enables the isolation of species that exhibit different structural motifs: the acetone fraction is dominated by island motifs, whereas Tol/THF/MeOH presents a higher abundance of archipelago species. Below, we demonstrate that the presence of archipelago motifs is critical in the production of water-soluble species by photo-oxidation of the asphaltene films.

## Visual Differences in the Weathering Products of the Asphaltene Films in a Solar Simulation Microcosm.

**Wyoming Deposit  $nC_7$  Asphaltenes****FIGURE 2****Athabasca Bitumen  $nC_7$  Asphaltenes**

**Figure 2.** Asphaltene films mixed with artificial seawater before and after irradiation in a solar simulation microcosm. Upper panel: whole Wyoming deposit  $nC_7$  asphaltenes and its acetone and Tol/THF/MeOH extrography fractions. Lower panel: whole Athabasca bitumen  $nC_7$  asphaltenes and its acetone and Tol/THF/MeOH extrography fractions.

**Table 1. Amount of Asphaltenes Loaded into the Solar Simulator and Water-Insoluble Material (Oil-Soluble Products + Precipitate) after the 24 h Irradiation Period**

sample	Wyoming deposit asphaltenes		sample	Athabasca bitumen asphaltenes	
	mass starting material (mg)	mass oil-soluble + precipitates (mg)		mass starting material (mg)	mass oil-soluble + precipitates (mg)
whole sample	19.9 ± 0.5	20.4 ± 0.2	whole sample	19.9 ± 0.6	17.0 ± 0.6
acetone fraction	20.0 ± 0.2	20.6 ± 0.5	acetone fraction	20.1 ± 0.3	18.1 ± 0.2
Tol/THF/MeOH fraction	20.0 ± 0.3	19.4 ± 0.4	Tol/THF/MeOH fraction	20.1 ± 0.4	16.6 ± 0.4

Figure 2 shows the physical appearance of the asphaltene films before and after photo-oxidation in a solar simulation microcosm. After the photo-oxidation of Wyoming deposit asphaltenes (upper panel), the artificial seawater appears colorless, and the remnant oil material reveals as a dark solid precipitate, either dispersed in the water or deposited at the bottom of the beaker. Conversely, the aqueous phase from

Athabasca bitumen asphaltenes (lower panel) has a dark yellow to brownish black color that suggests a significant production of dispersed solids and water-soluble species. Furthermore, the remnant oil phase, more evident for the acetone fraction, exhibits a brownish emulsion-like “mousse” consistency, similar to weathered samples observed after oil spills.<sup>53</sup> These results strongly suggest that the production of water-soluble com-

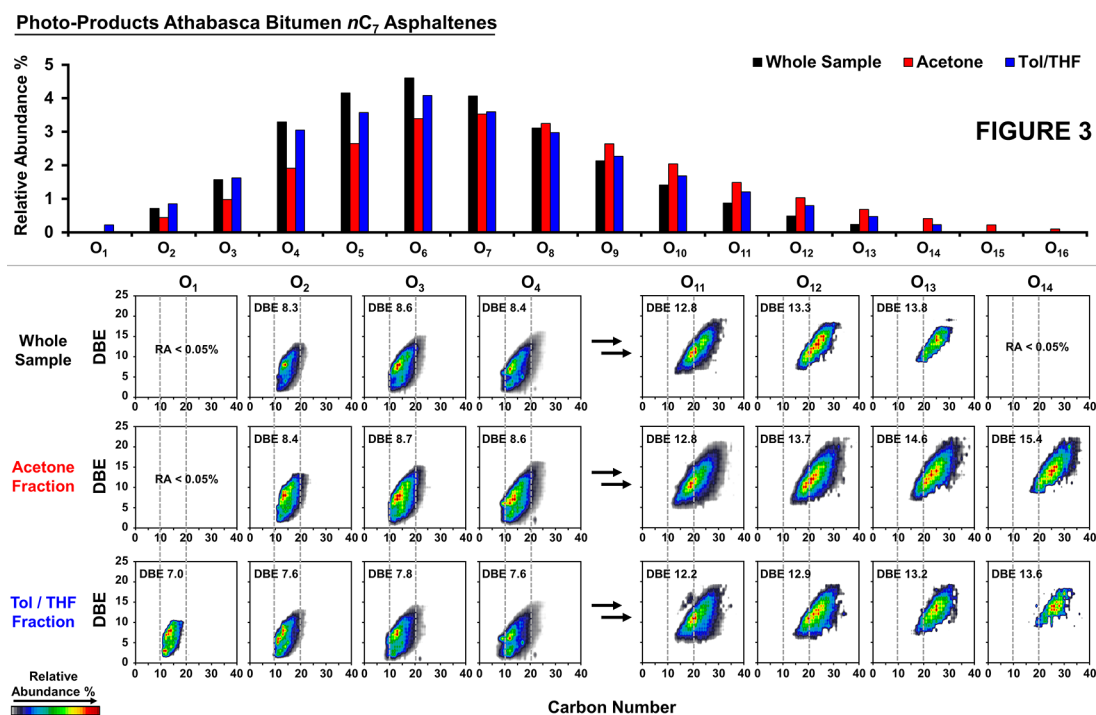


**Figure 3.** Heteroatom class distribution for  $O_1$ – $O_{16}$  species (upper panel) and corresponding isoabundance-contoured plots of DBE versus carbon number (lower panel) derived from (–) ESI 9.4 T FT-ICR MS analyses of water-soluble species from the photo-oxidation microcosm for Athabasca bitumen asphaltenes. Each plot indicates the average DBE value and the dotted lines define the approximate carbon number range.

pounds from the weathering processes of asphaltene-enriched feedstocks is sample-/structure-dependent.

Accurate evaluation of the amount of asphaltenes transferred into the aqueous phase is challenging because it requires quantification of the amount of oxygen incorporated during the simulated weathering processes. However, Table 1 presents the initial mass of asphaltenes loaded into the solar simulator and the mass of the water-insoluble material after the 24 h irradiation period (sum of oil-soluble products + precipitates). The gravimetric results suggest that Athabasca bitumen asphaltenes readily transform into water-soluble compounds. The amount of the water-insoluble material after photoirradiation of Wyoming asphaltenes is close to the quantity loaded into the solar simulator. We suspect that Wyoming deposit does not produce abundant water-soluble species, and the oil-soluble component increases in mass due to oxygen incorporation through photo-oxidation of the oil layer. However, further tests involving elemental analysis are required to confirm this suspicion and will be performed in a future study. On the other hand, the quantity of water insolubles for Athabasca asphaltenes, e.g., Tol/THF/MeOH fraction, indicates that at least ~15 wt % of the sample was transferred to the water. It is important to note that the Tol/THF/MeOH fraction is the most polar asphaltene extrography fraction. The increased polarity, as well as the higher content of multicore motifs, could explain their easier transformation into water-soluble compounds upon solar irradiation. Furthermore, it is critical to consider that asphaltene photo-oxidation in this work is likely a superficial process because the irradiated asphaltene solutions are dark, which decreases interactions with photons. Moreover, asphaltene aggregation might prevent some compounds being directly affected by solar irradiation, thereby limiting direct photo-oxidation to the asphaltene aggregate surface.

**Molecular Composition of Asphaltene-Derived  $O_x$  Water-Soluble Species.** Water-soluble organic species were extracted from water samples following laboratory irradiation by an SPE-PPL method, and molecular-level characterization was conducted by (–) ESI FT-ICR MS. As suggested by the cloudy/dark appearance of the aqueous phase after photo-oxidation, Athabasca bitumen asphaltenes produced a plethora of abundant water-soluble species as revealed by MS analysis (Figure 3). The number of assigned molecular formulas for the water-soluble extracts from whole Athabasca bitumen asphaltenes and its acetone and Tol/THF/MeOH extrography fractions were 10 042, 15 292, and 11 649, whereas the water-soluble extracts from whole Wyoming deposit asphaltenes and its acetone fraction did not reveal abundant mass spectral peaks consistent with the typical composition of DOM (only 105 and 507 molecular formulas were assigned). Therefore, this section focuses on the molecular composition of Athabasca bitumen water-soluble species. The water-soluble compounds from the Tol/THF/MeOH fraction from Wyoming deposit are discussed later.

Figure 3, upper panel, displays the heteroatom class distribution for water-soluble  $O_x$  species ( $x = 1$ – $16$ ) for whole Athabasca bitumen asphaltenes and its acetone and Tol/THF/MeOH extrography fractions (archipelago-dominant) and demonstrates the production of abundant, oxygen-enriched, water-soluble compounds, with up to 16 oxygen atoms. The molecular composition (DBE versus carbon number plots and van Krevelen diagrams of H/C versus O/C ratio<sup>54</sup>) and the number of assigned molecular formulas for the aqueous phase from the dark-control experiments (without solar irradiation) are presented in Supporting Information, Figure S1, and demonstrate the dominance of compound classes with low oxygen content (only up to four O atoms) without a well-defined compositional range. Therefore, photochemical reac-

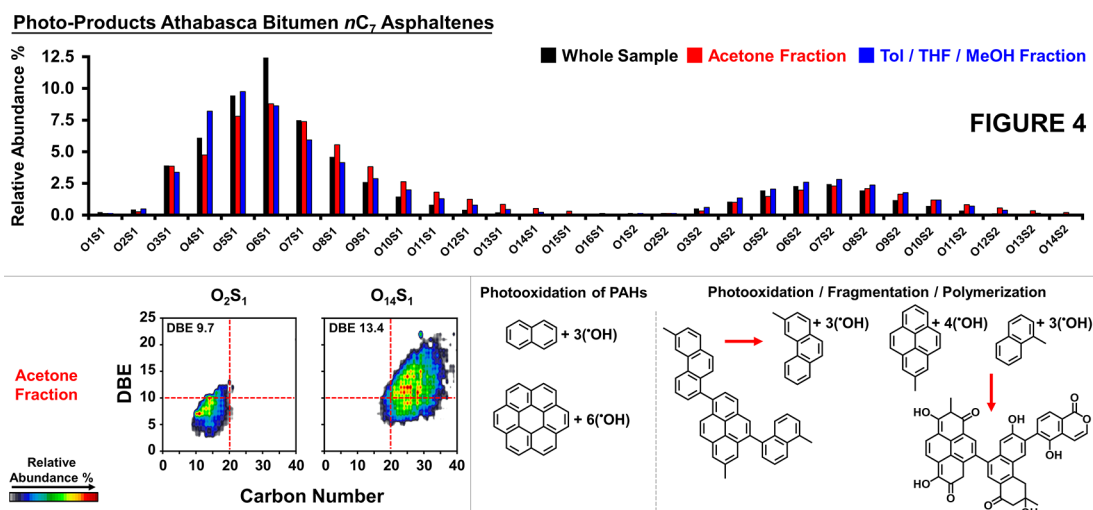


FIGURE 4

**Figure 4.** Heteroatom class distribution for O<sub>1</sub>S<sub>1</sub>–O<sub>15</sub>S<sub>1</sub> species (upper panel) and corresponding isoabundance-contoured plots of DBE versus carbon number (lower panel) derived from (–) ESI 9.4 T FT-ICR MS analyses of water-soluble species from the photo-oxidation microcosm for Athabasca bitumen asphaltenes. Each plot indicates the average DBE value and the dotted lines define the approximate carbon number range.

tions increase the number of oxygen atoms per molecule, even for the most refractory petroleum species, the asphaltenes, which become water soluble given their increased polarizability after photo-oxidation. However, asphaltene photo-oxidation reveals a strong structural dependence as suggested by the physical appearance of the water after irradiation of fractions enriched with different structural motifs (Figure 2). Supporting Information, Figure S2, shows the molecular composition of the SPE-PPL extracts from the aqueous phase collected after irradiation of whole Wyoming deposit asphaltenes and its acetone fraction (island-dominant). The results suggest that island-enriched samples are not suited for the production of petroleum-derived DOM, as indicated by the assignment of just a few molecular formulas (105 and 507 formulas), for low-order oxygen-containing species (O<sub>3</sub>–O<sub>7</sub>), without a well-defined/extended compositional range compared to the products from Athabasca bitumen.

Figure 3, lower panel, features color-contoured isoabundance plots of DBE versus carbon number for selected (for brevity) water-soluble O<sub>x</sub> species for whole Athabasca bitumen asphaltenes and its extrography fractions. DBE versus carbon number plots for all O<sub>x</sub> classes are included in Figure S3. Abundance-weighted DBE average values and vertical gray-dashed lines at carbon number 20 and 40 facilitate data visualization. First, for all samples, photo-oxidation produces O<sub>x</sub> species that occupy an extended compositional range between carbon number ~10–35 and DBE ~2–23. Second, the results demonstrate that the addition of one oxygen atom increases the overall abundance-weighted DBE by less than one value, as further shown in Supporting Information, Figure S4. The plots reveal linear trends between abundance-weighted DBE and the number of oxygen atoms, with slopes less than 1. These results suggest that photo-oxidation, in addition to incorporating ketone or aldehyde functionalities (the addition of one oxygen atom would increase the DBE by 1), as previously shown by Niles et al.,<sup>42</sup> can also add hydroxyl and carboxylic acid functionalities (addition of one oxygen atom with no DBE increase and two oxygen atoms with an increase in DBE of 1). Third, compound classes with high oxygen content (e.g., O<sub>13</sub> for Tol/THF/MeOH) contain ~10 additional carbon atoms than their oxygen-depleted counterparts (e.g., O<sub>3</sub> for Tol/THF/

MeOH). This result suggests that asphaltene photo-transformation may follow two plausible pathways. It is possible that photo-oxidized, low-carbon PAHs, generated through photo-fragmentation of multicore structures, may undergo addition reactions (polymerization) to produce oxygen-enriched species (e.g., O<sub>13</sub>) with higher DBE and carbon number. Another possible photo-oxidation pathway would be for high-molecular-weight PAHs, initially present in the starting material, to have the potential to incorporate more oxygen atoms than low-molecular-weight aromatic cores. The occurrence of photo-fragmentation and addition reactions (polymerization) in petroleum weathering is demonstrated below.

**Water-Soluble Sulfur-Containing Compounds.** Sulfur-containing compounds in dissolved organic matter (DOS) are critical for the global sulfur cycle because they comprise the largest organic sulfur reservoir in the ocean.<sup>55</sup> It is believed that the marine DOS pool consists of a small quantity of labile species that are rapidly recycled and generated by the abiotic incorporation of sulfur into DOM in sulfidic environments. However, a large portion of DOS consists of highly oxidized/refractory compounds, whose origin is poorly understood.<sup>33,50,56</sup> Because asphaltenes are refractory petroleum species that contain abundant sulfur functionalities, it is plausible that they serve as a potential source of stable DOS. Figure 4, upper panel, presents the heteroatom class distribution for water-soluble O<sub>x</sub>S<sub>y</sub> species (x = 1–15, y = 1–2) derived from the photo-oxidation of Athabasca bitumen asphaltenes. The results demonstrate that asphaltenes from all fractions generate abundant DOS with up to 15 oxygen atoms. Note that for the whole sample, which we have demonstrated to contain abundant archipelago motifs,<sup>40</sup> the relative abundance of the dominant O<sub>x</sub>S<sub>y</sub> class (O<sub>6</sub>S<sub>1</sub>) is ~2.5-fold higher than the dominant O<sub>x</sub> class (O<sub>6</sub>, Figure 3), suggesting that asphaltene samples that contain abundant archipelago motifs are a potential source of DOS. However, it is important to consider that asphaltenes from oil sand bitumens are sulfur rich; for instance, Athabasca bitumen nC<sub>7</sub> asphaltenes contain ~8.5 wt %.

The compositional range of O<sub>2</sub>S<sub>1</sub> and O<sub>14</sub>S<sub>1</sub> classes is highlighted in the lower panel of Figure 4. As observed for the O<sub>x</sub> continuum, asphaltene-derived DOS (O<sub>x</sub>S<sub>y</sub> species) also exhibits heavily oxidized species with ~2-fold carbon number

and much higher DBE (e.g.,  $O_{14}S_1$ , acetone fraction) than the oxygen-depleted counterparts for the same sample (e.g.,  $O_2S_1$ , acetone fraction). Figure 4, lower panel, illustrates the possible photochemical reaction pathways that yield species with increased oxygen content, higher carbon number, and higher DBE. First, high-molecular-weight aromatic cores, originally present in the starting material, would incorporate more oxygen atoms, as previously hypothesized for the model compounds.<sup>57–59</sup> Second, archipelago structures, also present in native asphaltenes, undergo photo-oxidation and photofragmentation to produce small/oxidized PAHs; such active species could experience polymerization to produce heavily oxidized (higher carbon number) water-soluble compounds. Figure 4, lower panel, highlights the generation of multicore motifs via addition reactions between oxygen-containing intermediate radicals. However, the addition of resonantly stabilized PAH radicals can also yield single-core compounds with higher molecular weight, as pointed out by Sinha et al. Our current efforts focus on understanding the structural motifs (single-core versus multicore) of the polymerization products.<sup>60</sup>

The DBE versus carbon number plots for all  $O_xS_1$  classes are included in Figure S5 and demonstrate that S-species with more than three oxygen atoms ( $>O_3S_1$ ) follow compositional trends similar to those for the  $O_x$  continuum (shown in Figure 3) because, as discussed above, the compositional range shifts to higher carbon number for  $O_xS_y$  species with an increased number of oxygen atoms. However, sulfur species with lower oxygen content do not follow the trend.  $O_1S_1$  and  $O_2S_1$  classes clearly contain abundant homologous series with DBE values of 7 and 9, which could correspond to the oxidized products from cycloalkyl/alkyl-substituted benzo- and dibenzo-thiophene species, well known for their high stability over geological time and stability under thermal cracking conditions.<sup>25,61</sup> Note that abundant homologous series with DBE values of 11 and 12 (whole sample, class  $O_1S_1$ , Figure S5) may correspond to the cycloalkyl/alkyl-substituted versions of highly stable thiophenic aromatic cores (dibenzo-/benzophtho-thiophene), in which oxygen might be incorporated as ketone, aldehyde, sulfoxide, or hydroxyl functionalities. Supporting Information, Figure S6, facilitates visualization of the suggested structures for the low-order oxidation products.

Moreover, Supporting Information, Figures S7–S9 present the compound class distribution and DBE versus carbon number plots for  $O_xS_2$ ,  $N_xO_y$ , and  $N_1O_xS_1$  water-soluble species, revealing trends similar to the  $O_x$  and  $O_xS_1$  classes. The results also support the hypothesis that sulfur compounds with lower oxygen content ( $O_3S_2$  class) exhibit abundant homologous series with DBE values consistent with possible stable cores (DBE = 6 and 9 for bithiophene and benzo-bithiophene, whose structures are also included in Supporting Information, Figure S6).

**Photofragmentation of Archipelago Motifs Produces Water-Soluble Species.** The dominance of island or archipelago motifs in petroleum asphaltenes determines their potential to produce small PAHs (one to five ring aromatics) upon thermal stress in refinery processes.<sup>40,62</sup> Figure 5 suggests that the dominance of a particular structural motif also determines asphaltene phototransformation products in the environment. Figure 5 presents the combined isoabundance-contoured plots of DBE versus carbon number for  $O_xS_1$  species for non-irradiated whole asphaltene samples and their extrography fractions (starting material) and their oil- and water-soluble phototransformation products. Figure 5 also

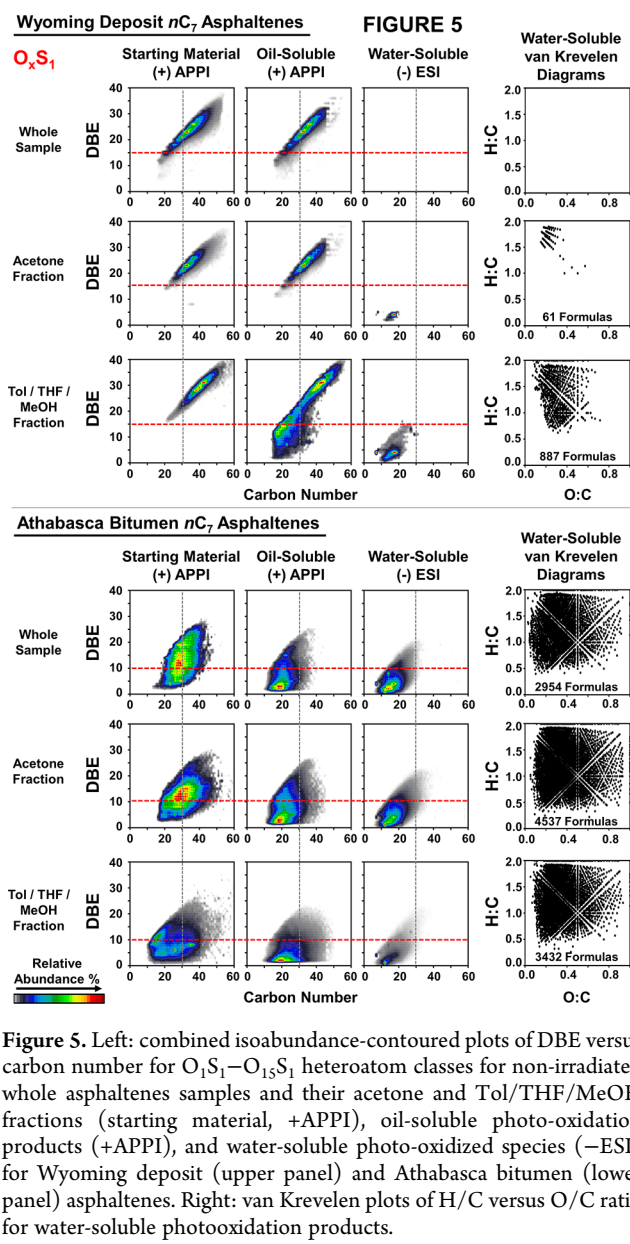


**Figure 5.** Left: combined isoabundance-contoured plots of DBE versus carbon number for  $O_1S_1$ – $O_{15}S_1$  heteroatom classes for non-irradiated whole asphaltene samples and their acetone and Tol/THF/MeOH fractions (starting material, +APPI), oil-soluble photo-oxidation products (+APPI), and water-soluble photo-oxidized species (–ESI) for Wyoming deposit (upper panel) and Athabasca bitumen (lower panel) asphaltenes. Right: van Krevelen plots of H/C versus O/C ratio for water-soluble photooxidation products.

includes the van Krevelen diagrams (H/C versus O/C ratio)<sup>54</sup> and the number of monoisotopic molecular formulas assigned for the water-soluble species. The results suggest that island motifs resist photoinduced fragmentation, because irradiation of whole Wyoming deposit asphaltenes and its acetone fraction (island-dominant), shown in Figure 5 upper panel, do not yield abundant water-soluble  $O_xS_1$  compounds with the typical compositional range of DOM (H/C  $\sim 0.5$ – $2$ , O/C  $\sim 0.2$ – $0.8$ ), as demonstrated by the van Krevelen diagrams.<sup>63</sup> Furthermore, their oil-soluble products resemble the compositional range of the starting material. However, the Tol/THF/MeOH fraction from Wyoming deposit, previously demonstrated to contain abundant archipelago motifs,<sup>40</sup> yields photo-oxidized oil-soluble compounds with a bimodal compositional range: the species with DBE  $> 15$  and carbon number  $> 30$  match the composition of the starting material, whereas the species with DBE  $< 15$  and carbon number  $< 30$  are likely archipelago-derived photofragmentation products. Furthermore, the Tol/THF/MeOH Wyoming species produce water-soluble com-

pounds that reside in a low-carbon number/typical compositional range of petroleum-derived.

Figure 5, lower panel, presents the compositional comparison for the starting material and the oil-/water-soluble products for Athabasca bitumen asphaltenes. Note that the compositional range of the starting material exhibits higher DBEs than the oil-/water-soluble products. The results suggest the occurrence of photofragmentation reactions through ring opening and/or cleavage of covalent bridges between aromatic cores in archipelago motifs; both processes contribute to the production of species with lower DBE values. Furthermore, the results point to a correlation between the degree of alkylation (carbon number) and partitioning of the oxidized species into water. The compositional range of the starting material and the oil-soluble products extends beyond carbon number 35, whereas most water-soluble species have carbon numbers between 10 and 20. Therefore, a higher alkylation degree (higher carbon number) decreases the solubility in water. The compositional trends for additional heteroatom groups support the notion that photofragmentation of the archipelago motifs is fundamental in the generation of DOM from asphaltene weathering ( $O_x$ ,  $O_xS_2$ , and  $N_1O_x$  species are shown in Supporting Information, Figures S10–S12).

**Petroleum Transformation by Sunlight Also Involves Polymerization.** To demonstrate that petroleum irradiation by sunlight can also promote polymerization reactions, a light distillate (178–283 °C) from an Arabian heavy oil sample was adsorbed onto silica gel and eluted with *n*-pentane to separate saturate/aromatic (nonpolar) species that were subsequently photo-oxidized in the solar simulation microcosm. The use of the nonpolar fraction from a light distillation cut ensures the dominance of low-carbon number species (<20) in the starting material. Therefore, any concurrent increase in carbon number (>20) and DBE upon photo-oxidation must result from addition reactions (polymerization). Figure 6 provides the compositional range for the saturate fraction from the light distillate (top) and the water-soluble oxidation products (bottom), accessed by negative-ion electrospray ionization coupled to FT-ICR MS. The starting material (upper panel) is lower in oxygen, because it contains only low abundant  $O_1$ ,  $O_2$ , and  $O_3$  classes that occupy a compositional range with DBE values below 10 and carbon numbers between 10 and 20. Figure 6, lower panel, demonstrates that photo-oxidation yields water-soluble compounds with up to 12 oxygen atoms with a more extended compositional range in terms of carbon number and DBE. Oxygen-depleted species (e.g.,  $O_{11}$ ,  $O_2$ , and  $O_3$  classes) remain in the compositional range of the starting material, whereas heavily oxidized compounds (> $O_8$ ) exhibit twice the DBE and carbon number values. Although the increase in DBE suggests that oxygen may be incorporated as carbonyl functionalities, the concurrent increase of carbon number is possible only if polymerization (addition reactions) has occurred. Therefore, the results demonstrate that petroleum compounds can experience polymerization reactions during solar irradiation. In particular, polymerization was shown for a distillate cut with a narrow compositional range, and this process should not be simply extrapolated to samples with a wider carbon number and DBE range, like asphaltenes. However, it is important to note that the compositional range for oxygen-enriched classes ( $O_x > O_{10}$ ) derived from the Arabian distillate extends beyond carbon number 30, similar to heavily oxidized water-soluble asphaltene products. Thus, combined with the compositional trends for asphaltene photo-oxidation/photofragmentation, these results

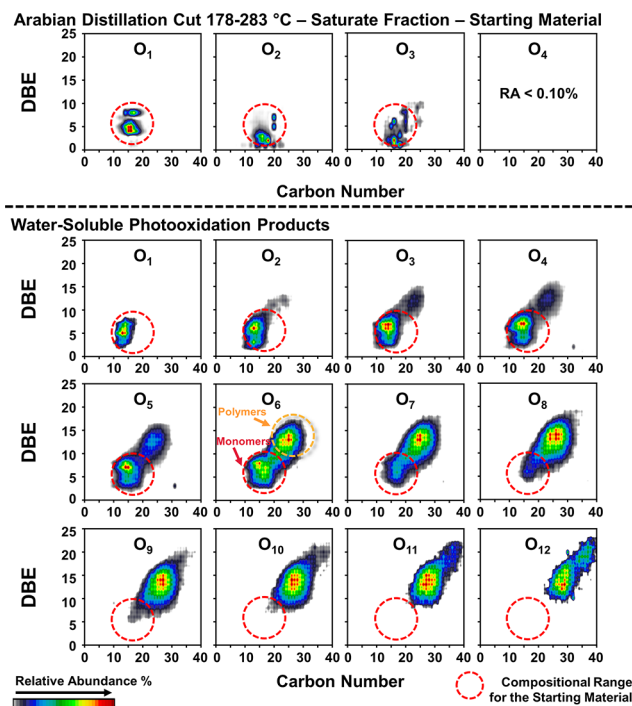


**Figure 6.** Isoabundance-contoured plots of DBE versus carbon number for  $O_x$  compound classes for the saturates/nonpolar fraction from an Arabian heavy boiling cut (178–283 °C) and its water-soluble photo-oxidation products. Data derived from (–) ESI 9.4 T FT-ICR MS.

suggest a possible pathway for the transformation of large/alkyl-enriched archipelago asphaltene species. We hypothesize that simultaneous photo-oxidation and photofragmentation increase oxygen content and decrease molecular size. Subsequently, low-carbon number/oxidized photoactivated species undergo polymerization and produce heavily oxidized compounds with higher carbon number and higher DBE. Additional experimental evidence for the existence of polymerization in asphaltenes is needed and should address the possible occurrence of addition reactions between sulfide moieties (R–S–R') for sulfur-enriched oils such as Athabasca bitumen and South American crudes, as previously shown in the geochemistry studies by Silva et al.<sup>64</sup>

**Implications for Future Studies.** Two asphaltene samples were separated into fractions enriched with different structural motifs, island or archipelago, and photo-oxidized in a solar simulator microcosm. The results demonstrate that highly aromatic asphaltene samples, with dominant island structure, resist photofragmentation and yield limited water-soluble species as detected by mass spectrometry. Conversely, asphaltene samples enriched in archipelago structural motifs yield abundant water-soluble species with a molecular composition characteristic of petroleum-derived dissolved organic matter. The compositional range of the oil-/water-soluble photo-oxidation products suggests that photofragmentation of archipelago motifs is central in the transformation of asphaltenes into DOM/DOS. Finally, the photo-oxidation of petroleum species with a fixed carbon number range (10–20) and DBE (<10) yields water-soluble compounds with ~2-fold carbon number and DBE increase, which suggests that polymerization reactions are involved in petroleum photo-transformation. The results highlight that petroleum degradation by sunlight involves three concerted processes: photo-

oxidation, photofragmentation, and polymerization. The importance of each in the long-term fate of weathered petroleum is currently unknown and will require longer time period photomicrocosms (to capture both oil- and water-soluble products) and comparison to field samples. However, the present results suggest that it is strongly linked to the molecular structure, which will be the subject of continued research.

## ■ ASSOCIATED CONTENT

### Supporting Information

The Supporting Information is available free of charge at <https://pubs.acs.org/doi/10.1021/acs.est.0c01158>.

Compositional range for the water-soluble fraction from the dark controls for whole Athabasca bitumen C<sub>7</sub> asphaltenes and its acetone and Tol/THF/MeOH fraction (−ESI 9.4 T FT-ICR MS) (Figure S1) (PDF)

Compositional range for the water-soluble fraction from the photo-oxidation of whole Wyoming deposit C<sub>7</sub> asphaltenes and its acetone fraction (−ESI 9.4 T FT-ICR MS) (Figure S2) (PDF)

Class distribution (upper panel) and contoured plots of DBE versus carbon number (lower panel) for O<sub>x</sub> species derived from (−) ESI 9.4 T FT-ICR MS analyses of water-soluble species from the photo-oxidation of Athabasca bitumen asphaltenes (Figure S3) (PDF)

Trendlines for abundance-weighted DBE versus number of oxygen atoms for O<sub>x</sub> and O<sub>x</sub>S<sub>1</sub> water-soluble species for Athabasca bitumen asphaltenes (Figure S4) (PDF)

Class distribution (upper panel) and contoured plots of DBE versus carbon number (lower panel) for O<sub>x</sub>S<sub>1</sub> species derived from (−) ESI 9.4 T FT-ICR MS analyses of water-soluble species from the photo-oxidation of Athabasca bitumen asphaltenes (Figure S5) (PDF)

Suggested structures for stable aromatic cores for low-order oxygen-containing water-soluble S-compounds (Figure S6) (PDF)

Class distribution for O<sub>x</sub>S<sub>y</sub> species (upper panel) and respective contoured plots of DBE versus carbon number (lower panel) derived from (−) ESI 9.4 T FT-ICR MS analyses of water-soluble species from the photo-oxidation of Athabasca bitumen asphaltenes (Figure S7) (PDF)

Class distribution for N<sub>x</sub>O<sub>y</sub> and N<sub>1</sub>O<sub>x</sub>S<sub>1</sub> species (upper panel) and contoured plots of DBE versus carbon number (lower panel) for N<sub>1</sub>O<sub>y</sub> classes derived from (−) ESI 9.4 T FT-ICR MS analyses of water-soluble species from the photo-oxidation of Athabasca bitumen asphaltenes (Figure S8) (PDF)

Class distribution for N<sub>x</sub>O<sub>y</sub> and N<sub>1</sub>O<sub>x</sub>S<sub>1</sub> species (upper panel) and contoured plots of DBE versus carbon number (lower panel) for N<sub>2</sub>O<sub>y</sub> and N<sub>1</sub>O<sub>x</sub>S<sub>1</sub> classes derived from (−) ESI 9.4 T FT-ICR MS analyses of water-soluble species from the photo-oxidation of Athabasca bitumen asphaltenes (Figure S9) (PDF)

Combined contoured plots of DBE versus carbon number for O<sub>x</sub> compound classes for non-irradiated whole asphaltene samples and their acetone and Tol/THF/MeOH fractions (starting material, +APPI), oil-soluble oxidation products (+APPI), and water-soluble oxidized species (−ESI) for Wyoming deposit (left panel) and Athabasca bitumen (right panel) asphaltenes. Van Krevelen diagrams and the number of assigned formulas

for water-soluble O<sub>x</sub> species are also included (Figure S10) (PDF)

Combined contoured plots of DBE versus carbon number for O<sub>x</sub>S<sub>2</sub> compound classes for non-irradiated whole asphaltenes samples and their acetone and Tol/THF/MeOH fractions (starting material, +APPI), oil-soluble oxidation products (+APPI), and water-soluble oxidized species (−ESI) for Wyoming deposit (upper panel) and Athabasca bitumen (lower panel) asphaltenes (Figure S11) (PDF)

Combined contoured plots of DBE versus carbon number for N<sub>x</sub>O<sub>y</sub> compound classes for non-irradiated whole asphaltenes samples and their acetone and Tol/THF/MeOH fractions (starting material, +APPI), oil-soluble oxidation products (+APPI), and water-soluble oxidized species (−ESI) for Wyoming deposit (upper panel) and Athabasca bitumen (lower panel) asphaltenes (Figure S12) (PDF)

## ■ AUTHOR INFORMATION

### Corresponding Authors

**Martha L. Chacón-Patiño** – Department of Chemistry and Biochemistry, Florida State University, Tallahassee, Florida 32308, United States; [orcid.org/0000-0002-7273-5343](https://orcid.org/0000-0002-7273-5343); Email: [chacon@magnet.fsu.edu](mailto:chacon@magnet.fsu.edu)

**Ryan P. Rodgers** – Ion Cyclotron Resonance Program, National High Magnetic Field Laboratory and Department of Chemistry and Biochemistry, Florida State University, Tallahassee, Florida 32310, United States; [orcid.org/0000-0003-1302-2850](https://orcid.org/0000-0003-1302-2850); Phone: +1 850-644-2398; Email: [rodders@magnet.fsu.edu](mailto:rodders@magnet.fsu.edu)

### Authors

**Sydney F. Niles** – Ion Cyclotron Resonance Program, National High Magnetic Field Laboratory and Department of Chemistry and Biochemistry, Florida State University, Tallahassee, Florida 32310, United States; [orcid.org/0000-0002-3487-6612](https://orcid.org/0000-0002-3487-6612)

**Alan G. Marshall** – Ion Cyclotron Resonance Program, National High Magnetic Field Laboratory and Department of Chemistry and Biochemistry, Florida State University, Tallahassee, Florida 32310, United States; [orcid.org/0000-0001-9375-2532](https://orcid.org/0000-0001-9375-2532)

**Christopher L. Hendrickson** – Ion Cyclotron Resonance Program, National High Magnetic Field Laboratory and Department of Chemistry and Biochemistry, Florida State University, Tallahassee, Florida 32310, United States

Complete contact information is available at: <https://pubs.acs.org/doi/10.1021/acs.est.0c01158>

### Notes

The authors declare no competing financial interest.

## ■ ACKNOWLEDGMENTS

This research was made possible in part by a grant from The Gulf of Mexico Research Initiative. Work was performed at the National High Magnetic Field Laboratory ICR User Facility, which is supported by the National Science Foundation Division of Chemistry through Cooperative Agreement DMR-1644779 and the State of Florida. The authors thank Greg T. Blakney for help with data calibration and Yuri E. Corilo for PetroOrg software.<sup>45</sup>

## ■ REFERENCES

- (1) Ismail, Z.; Karim, R. Some Technical Aspects of Spills in the Transportation of Petroleum Materials by Tankers. *Saf. Sci.* **2013**, *51*, 202–208.
- (2) Stiver, W.; Mackay, D. Evaporation Rate of Spills of Hydrocarbons and Petroleum Mixtures. *Environ. Sci. Technol.* **1984**, *18*, 834–840.
- (3) National Research Council (US) Committee on Oil in the Sea: Inputs, Fates, and Effects. Behavior and Fate of Oil. *Oil in the Sea III: Inputs, Fates, and Effects*; National Academies Press: Washington, D.C., 1999; Chapter 4, pp 89–265.
- (4) Ward, C. P.; Overton, E. B. How the 2010 Deepwater Horizon Spill Reshaped Our Understanding of Crude Oil Photochemical Weathering at Sea: A Past, Present, and Future Perspective. *Environ. Sci.: Processes Impacts* **2020**, 1125–1138.
- (5) Warnock, A. M.; Hagen, S. C.; Passeri, D. L. Marine Tar Residues: A Review. *Water, Air, Soil Pollut.* **2015**, *226*, No. 68.
- (6) Lewan, M. D.; Warden, A.; Dias, R. F.; Lowry, Z. K.; Hannah, T. L.; Lillis, P. G.; Kokaly, R. F.; Hoefen, T. M.; Swayze, G. A.; Mills, C. T.; Harris, S. H.; Plumlee, G. S. Asphaltene Content and Composition as a Measure of Deepwater Horizon Oil Spill Losses within the First 80 days. *Org. Geochem.* **2014**, *75*, 54–60.
- (7) Chacón-Patiño, M. L.; Rowland, S. M.; Rodgers, R. P. Advances in Asphaltene Petroleomics. Part 1: Asphaltenes Are Composed of Abundant Island and Archipelago Structural Motifs. *Energy Fuels* **2017**, *31*, 13509–13518.
- (8) Qiao, P.; Harbottle, D.; Tchoukov, P.; Masliyah, J.; Sjoblom, J.; Liu, Q.; Xu, Z. Fractionation of Asphaltenes in Understanding Their Role in Petroleum Emulsion Stability and Fouling. *Energy Fuels* **2017**, *31*, 3330–3337.
- (9) Spiecker, P. M.; Kilpatrick, P. K. Interfacial Rheology of Petroleum Asphaltenes at the Oil-Water Interface. *Langmuir* **2004**, *20*, 4022–4032.
- (10) Bobra, M.; Fingas, M.; Tennyson, E. *When Oil Spills Emulsify*; CHEMTECH, ACS, 1992; Vol. 22, pp 236–241.
- (11) Gawrys, K. L.; Spiecker, P. M.; Kilpatrick, P. K. The Role of Asphaltene Solubility and Chemical Composition on Asphaltene Aggregation. *Pet. Sci. Technol.* **2003**, *21*, 461–489.
- (12) Schuler, B.; Meyer, G.; Peña, D.; Mullins, O. C.; Gross, L. Unraveling the Molecular Structures of Asphaltenes by Atomic Force Microscopy. *J. Am. Chem. Soc.* **2015**, *137*, 9870–9876.
- (13) Gray, M.; Tykwinski, R.; Stryker, J.; Tan, X. Supramolecular Assembly Model for Aggregation of Petroleum Asphaltenes. *Energy Fuels* **2011**, *25*, 3125–3134.
- (14) Buckley, J. S. Asphaltene Deposition. *Energy Fuels* **2012**, *26*, 4086–4090.
- (15) Yasar, M.; Trauth, D. M.; Klein, M. T. Asphaltene and Resid Pyrolysis. 2. The Effect of Reaction Environment on Pathways and Selectivities. *Energy Fuels* **2001**, *15*, 504–509.
- (16) Lehr, W.; Jones, R.; Evans, M.; Simecek-Beatty, D.; Overstreet, R. Revisions of the ADIOS Oil Spill Model. *Environ. Model. Software* **2002**, *17*, 189–197.
- (17) Kumbarger, Y. S.; Biligiri, K. P. Understanding Aging Behaviour of Conventional Asphalt Binders Used in India. *Transp. Res. Procedia* **2016**, *17*, 282–290.
- (18) Speight, J. G. Asphalt Paving. *Asph. Mater. Sci. Technol.* **2016**, 409–435.
- (19) Huang, B.; Li, G.; Vukosavljevic, D.; Shu, X.; Egan, B. K. Laboratory Investigation of Mixing Hot-Mix Asphalt with Reclaimed Asphalt Pavement. *Transp. Res. Rec.* **2005**, *1929*, 37–45.
- (20) Azizian, M. F.; Nelson, P. O.; Thayumanavan, P.; Williamson, K. J. Environmental Impact of Highway Construction and Repair Materials on Surface and Ground Waters: Case Study. Crumb Rubber Asphalt Concrete. *Waste Manage.* **2003**, *23*, 719–728.
- (21) Mahler, B. J.; Van Metre, P. C.; Foreman, W. T. Concentrations of Polycyclic Aromatic Hydrocarbons (PAHs) and Azaarenes in Runoff from Coal-Tar- and Asphalt-Sealcoated Pavement. *Environ. Pollut.* **2014**, *188*, 81–87.
- (22) Haas, E.; Ericson, C. L.; Bennert, T. Laboratory Designed Hot Mix Asphalt Mixtures with Post-Consumer Recycled Asphalt Shingles (RAS) Utilizing AASHTO PP78. *Constr. Build. Mater.* **2019**, *226*, 662–672.
- (23) Lin, M. S.; Lunsford, K. M.; Glover, C. J.; Davison, R. R.; Bullin, J. A. The Effects of Asphaltenes on the Chemical and Physical Characteristics of Asphalt. *Asphaltenes* **1995**, 155–176.
- (24) Chacón-Patiño, M. L.; Rowland, S. M.; Rodgers, R. P. The Compositional and Structural Continuum of Petroleum from Light Distillates to Asphaltenes: The Boduszynski Continuum Theory as Revealed by FT-ICR Mass Spectrometry. In *The Boduszynski Continuum: Contributions to the Understanding of the Molecular Composition of Petroleum*; Ovalles, C.; Moir, M. E., Eds.; ACS Symposium Series; ACS: Washington, D.C., 2018; Vol. 1282, pp 113–171.
- (25) Chacón-Patiño, M. L.; Blanco-Tirado, C.; Orrego-Ruiz, J. A.; Gómez-Escudero, A.; Combariza, M. Y. Tracing the Compositional Changes of Asphaltenes after Hydroconversion and Thermal Cracking Processes by High-Resolution Mass Spectrometry. *Energy Fuels* **2015**, *29*, 6330–6341.
- (26) Brandt, H. C. A.; de Groot, P. C. Aqueous Leaching of Polycyclic Aromatic Hydrocarbons from Bitumen and Asphalt. *Water Res.* **2001**, *35*, 4200–4207.
- (27) Xue, Y.; Hu, Z.; Wang, C.; Xiao, Y. Evaluation of Dissolved Organic Carbon Released from Aged Asphalt Binder in Aqueous Solution. *Constr. Build. Mater.* **2019**, *218*, 465–476.
- (28) Hallberg, M.; Renman, G.; Lundbom, T. Seasonal Variations of Ten Metals in Highway Runoff and Their Partition between Dissolved and Particulate Matter. *Water, Air, Soil Pollut.* **2007**, *181*, 183–191.
- (29) Zhao, C.; Wang, C. C.; Li, J. Q.; Wang, C. Y.; Wang, P.; Pei, Z. J. Dissolved Organic Matter in Urban Stormwater Runoff at Three Typical Regions in Beijing: Chemical Composition, Structural Characterization and Source Identification. *RSC Adv.* **2015**, *5*, 73490–73500.
- (30) Norin, M.; Strömvaix, A. M. Leaching of Organic Contaminants from Storage of Reclaimed Asphalt Pavement. *Environ. Technol.* **2004**, *25*, 323–340.
- (31) Sansalone, J. J.; Buchberger, S. G.; Al-Abed, S. R. Fractionation of Heavy Metals in Pavement Runoff. *Sci. Total Environ.* **1996**, *189–190*, 371–378.
- (32) Hertkorn, N.; Harir, M.; Cawley, K. M.; Schmitt-Kopplin, P.; Jaffé, R. Molecular Characterization of Dissolved Organic Matter from Subtropical Wetlands: A Comparative Study through the Analysis of Optical Properties, NMR and FTICR/MS. *Biogeosciences* **2016**, *13*, 2257–2277.
- (33) Ksionzek, K. B.; Lechtenfeld, O. J.; McCallister, S. L.; Schmitt-Kopplin, P.; Geuer, J. K.; Geibert, W.; Koch, B. P. Dissolved Organic Sulfur in the Ocean: Biogeochemistry of a Petagram Inventory. *Science* **2016**, *354*, 456–459.
- (34) Birgisdóttir, H.; Gamst, J.; Christensen, T. H. Leaching of PAHs from Hot Mix Asphalt Pavements. *Environ. Eng. Sci.* **2007**, *24*, 1409–1421.
- (35) Scheepers, P. T. J.; Bos, R. P. Environmental Health Review Articles Combustion of Diesel Fuel from a Toxicological Perspective I Origin of Incomplete Combustion Products. *Int. Arch. Occup. Environ. Health* **1992**, *64*, 149–161.
- (36) Mullins, O. C.; Sabbah, H.; Eyssautier, J.; Pomerantz, A. E.; Barre', L.; Andrews, A. B.; Ruiz-Morales, Y.; Mostowfi, F.; McFarlane, R.; Goual, L.; Lepkowitz, R.; Cooper, T.; Orbulescu, J.; Leblanc, R. M.; Edwards, J.; Zare, R. N. Advances in Asphaltene Science and the Yen–Mullins Model. *Energy Fuels* **2012**, *26*, 3986–4003.
- (37) Riedeman, J. S.; Kadasala, N. R.; Wei, A.; Kenttämaa, H. I. Characterization of Asphaltene Deposits by Using Mass Spectrometry and Raman Spectroscopy. *Energy Fuels* **2016**, *30*, 805–809.
- (38) Sabbah, H.; Morrow, A. L.; Pomerantz, A. E.; Zare, R. N. Evidence for Island Structures as the Dominant Architecture of Asphaltenes. *Energy Fuels* **2011**, *25*, 1597–1604.
- (39) Chacón-Patiño, M. L.; Rowland, S. M.; Rodgers, R. P. Advances in Asphaltene Petroleomics. Part 2: Selective Separation Method That Reveals Fractions Enriched in Island and Archipelago Structural Motifs by Mass Spectrometry. *Energy Fuels* **2018**, *32*, 314–328.

- (40) Chacón-Patiño, M. L.; Rowland, S. M.; Rodgers, R. P. Advances in Asphaltene Petroeomics. Part 3. Dominance of Island or Archipelago Structural Motif Is Sample Dependent. *Energy Fuels* **2018**, *32*, 9106–9120.
- (41) Nyadong, L.; Lai, J.; Thompsen, C.; LaFrancois, C. J.; Cai, X.; Song, C.; Wang, J.; Wang, W. High-Field Orbitrap Mass Spectrometry and Tandem Mass Spectrometry for Molecular Characterization of Asphaltenes. *Energy Fuels* **2018**, *32*, 294–305.
- (42) Niles, S. F.; Chacón-Patiño, M. L.; Chen, H.; McKenna, A. M.; Blakney, G. T.; Rodgers, R. P.; Marshall, A. G. Molecular-Level Characterization of Oil-Soluble Ketone/Aldehyde Photo-Oxidation Products by Fourier Transform Ion Cyclotron Resonance Mass Spectrometry Reveals Similarity Between Microcosm and Field Samples. *Environ. Sci. Technol.* **2019**, *53*, 6887–6894.
- (43) Ward, C. P.; Sharpless, C. M.; Valentine, D. L.; French-McCay, D. P.; Aeppli, C.; White, H. K.; Rodgers, R. P.; Gosselin, K. M.; Nelson, R. K.; Reddy, C. M. Partial Photochemical Oxidation Was a Dominant Fate of Deepwater Horizon Surface Oil. *Environ. Sci. Technol.* **2018**, *52*, 1797–1805.
- (44) King, S. M.; Leaf, P. A.; Olson, A. C.; Ray, P. Z.; Tarr, M. A. Photolytic and Photocatalytic Degradation of Surface Oil from the Deepwater Horizon Spill. *Chemosphere* **2014**, *95*, 415–422.
- (45) Overton, E. B.; Laseter, J. L.; Mascarella, S. W.; Raschke, C.; Nuiry, I.; Farrington, J. W. In *Photochemical Oxidation of IXTOC I Oil*, Symposium on Preliminary Results from the September 1979 Researcher/Pierce IXTOC I Cruise, Key Biscayne, Florida, 1980; pp 341–383.
- (46) Chacón-Patiño, M. L.; Vesga-Martínez, S. J.; Blanco-Tirado, C.; Orrego-Ruiz, J. A.; Gómez-Escudero, A.; Combariza, M. Y. Exploring Occluded Compounds and Their Interactions with Asphaltene Networks Using High-Resolution Mass Spectrometry. *Energy Fuels* **2016**, *30*, 4550–4561.
- (47) Dittmar, T.; Koch, B.; Hertkorn, N.; Kattner, G. A Simple and Efficient Method for the Solid-Phase Extraction of Dissolved Organic Matter (SPE-DOM) from Seawater. *Limnol. Oceanogr. Methods* **2008**, *6*, 230–235.
- (48) Kaiser, N. K.; Quinn, J. P.; Blakney, G. T.; Hendrickson, C. L.; Marshall, A. G. A Novel 9.4 Tesla FTICR Mass Spectrometer with Improved Sensitivity, Mass Resolution, and Mass Range. *J. Am. Soc. Mass Spectrom.* **2011**, *22*, 1343–1351.
- (49) Purcell, J. M.; Merdrignac, I.; Rodgers, R. P.; Marshall, A. G.; Gauthier, T.; Guibard, I. Stepwise Structural Characterization of Asphaltenes during Deep Hydroconversion Processes Determined by Atmospheric Pressure Photoionization (APPI) Fourier Transform Ion Cyclotron Resonance (FT-ICR) Mass Spectrometry. *Energy Fuels* **2010**, *24*, 2257–2265.
- (50) Gomez-Saez, G. V.; Pohlbeln, A. M.; Stubbins, A.; Marsay, C. M.; Dittmar, T. Photochemical Alteration of Dissolved Organic Sulfur from Sulfidic Porewater. *Environ. Sci. Technol.* **2017**, *51*, 14144–14154.
- (51) Blakney, G. T.; Hendrickson, C. L.; Marshall, A. G. Predator Data Station: A Fast Data Acquisition System for Advanced FT-ICR MS Experiments. *Int. J. Mass Spectrom.* **2011**, *306*, 246–252.
- (52) Corilo, Y. E. *PetroOrg Software*; Florida State University, 2013.
- (53) Liu, Z.; Liu, J.; Zhu, Q.; Wu, W. The Weathering of Oil after the DeepwaterHorizon Oil Spill: Insights from the Chemical Composition of the Oil from the Sea Surface, Salt Marshes and Sediments. *Environ. Res. Lett.* **2012**, *7*, No. 035302.
- (54) Wu, Z.; Rodgers, R. P.; Marshall, A. G. Two- and Three-Dimensional van Krevelen Diagrams: A Graphical Analysis Complementary to the Kendrick Mass Plot for Sorting Elemental Compositions of Complex Organic Mixtures Based on Ultrahigh-Resolution Broadband Fourier Transform Ion Cyclotron Resonance. *Anal. Chem.* **2004**, *76*, 2511–2516.
- (55) Houle, D.; Carignan, R.; Lachance, M.; DuPont, J. Dissolved Organic Carbon and Sulfur in Southwestern Quebec Lakes: Relationships with Catchment and Lake Properties. *Limnol. Oceanogr.* **1995**, *40*, 710–717.
- (56) Pohlbeln, A. M.; Dittmar, T. Novel Insights into the Molecular Structure of Non-Volatile Marine Dissolved Organic Sulfur. *Mar. Chem.* **2015**, *168*, 86–94.
- (57) McConkey, B. J.; Hewitt, L. M.; Dixon, D. G.; Greenberg, B. M. Natural Sunlight Induced Photooxidation of Naphthalene in Aqueous Solution. *Water, Air, Soil Pollut.* **2002**, *136*, 347–359.
- (58) Ehrenhauser, F. S. *Photochemical Reaction Products of Polycyclic Aromatic Hydrocarbons Adsorbed at an Air-Water Interface Photochemical Reaction Products Air–Water Interface*; Louisiana State University, 2011.
- (59) Rojas, L.; Peraza, A.; Ruetter, F. Aging Oxidation Reactions on Atmospheric Black Carbon by OH Radicals. A Theoretical Modeling Study. *J. Phys. Chem. A* **2015**, *119*, 13038–13047.
- (60) Glattko, T. J.; Patiño, M. L. C.; Niles, S. F.; Hendrickson, C. L.; Marshall, A. G.; Rodgers, R. P. *FT-ICR MS Reveals the Structural Dependence of Emerging and Recalcitrant Contaminants Generated from the Widespread Use of Natural Products*, 68th ASMS Annual Conference Mass Spectrometry & Allied Topics, May 31–June 4, 2020; Poster TP 151.
- (61) Rueda-Velásquez, R. I.; Freund, H.; Qian, K.; Olmstead, W. N.; Gray, M. R. Characterization of Asphaltene Building Blocks by Cracking under Favorable Hydrogenation Conditions. *Energy Fuels* **2013**, *27*, 1817–1829.
- (62) Karimi, A.; Qian, K.; Olmstead, W. N.; Freund, H.; Yung, C.; Gray, M. R. Quantitative Evidence for Bridged Structures in Asphaltenes by Thin Film Pyrolysis. *Energy Fuels* **2011**, *25*, 3581–3589.
- (63) Stubbins, A.; Spencer, R. G. M.; Chen, H.; Hatcher, P. G.; Mopper, K.; Hernes, P. J.; Mwamba, V. L.; Mangangu, A. M.; Wabakanghanzi, J. N.; Six, J. Illuminated Darkness: Molecular Signatures of Congo River Dissolved Organic Matter and Its Photochemical Alteration as Revealed by Ultrahigh Precision Mass Spectrometry. *Limnol. Oceanogr.* **2010**, *55*, 1467–1477.
- (64) Silva, R. C.; Yim, C.; Radović, J. R.; Brown, M.; Weerawardhena, P.; Huang, H.; Snowdon, L. R.; Oldenburg, T. B. P.; Larter, S. R. Mechanistic Insights into Sulfur Rich Oil Formation, Relevant to Geological Carbon Storage Routes. A Study Using (+) APPI FTICR-MS Analysis. *Org. Geochem.* **2020**, *147*, 1–14.